Optical magnon sidebands and exciton dynamics in the two-dimensional antiferromagnet $BaMnF_4$ at $T=2$ K

R. Moncorgé, B. Jacquier, and R. Mahiou
Laboratoire de Physico-Chimie des Matériaux Luminescents du Centre National de la Recherche Scientifique, Université de Lyon I, F-69622 Villeurbanne, France

C. Uihlein
Max Planck Institute, Grenoble, France
(Received 17 October 1983)

Our previous observations of pure exciton and magnon-assisted optical transitions in the $^4T_1(^4G)$ state of Mn^{2+} ions in the layer-type antiferromagnet $BaMnF_4$ are analyzed in detail. The magnon density of states and the line profiles of the one-magnon sidebands are calculated with the adoption of a model in which only exchange interactions within the sheets perpendicular to the b axis are considered. The fits to the data allow us to obtain values of the exchange integrals J_1 and J_2 between near-neighbor Mn^{2+} ions along the a and c directions of the crystal in very close agreement with those obtained from neutron-diffraction data. In addition, distortion of the magnetic structure by the application of a strong magnetic field is shown to act directly on the exciton dynamics; it confirms its quasilocalized character at zero field as well as the exchange nature of the interionic interactions which allow the exciton to migrate in the crystal when the external field is switched on.

I. INTRODUCTION

In antiferromagnetic manganese compounds the excitonic excitations come from elementary optical transitions within the manganese ions for which the spin projection changes by unity. Thus when the interionic interactions responsible for the collective nature of these excitations is dominated by exchange or superexchange coupling, the so-called Frenkel excitons can migrate only among ferromagnetically coupled manganese ions.[1] Since the exchange is short range, this spin selection rule may confine the excitons to well-defined planes or chains of magnetic ions depending upon the crystallomagnetic structure.

A number of works have appeared more or less recently on the optical properties of the one-dimensional antiferromagnets such as $(CH_3)_4NMnCl_3$ (TMMC),[2] $CsMnBr_3$ (CMB),[3] or $CsMnCl_3\cdot 2H_2O$ (CMC).[4,5] In agreement with the above rule, all of these studies indicate a quasicomplete self-localization of the optical excitations. Much less attention has been addressed thus far to the characteristics of the exciton dynamics in the two-dimensional compounds.

In an earlier paper, we reported on very new fluorescence results obtained on the layer-type antiferromagnet $BaMnF_4$ at low temperature.[6] We presented our observations of optical structures in the region of the pure exciton state $^4T_{1g}(^4G)$ of the Mn^{2+} ions. Some of them were tentatively assigned to pure excitons and the others to magnon-assisted transitions. In agreement with the crystallomagnetic structure, preliminary results on the time evolution of the various fluorescence features indicated, as in the one-dimensional systems, a quasicomplete localization of the excitons.

We present now a calculation of the magnon density of states and of the corresponding exciton-magnon line shapes which are expected in emission as well as in absorption. These theoretical results are compared with the experimental data to ascertain our primary attributions and to show the importance of exchange coupling in the interionic interactions. The dynamical properties of the system are reached through the analysis of the effect of an applied magnetic field.

II. PRELIMINARY INFORMATION AND EXPERIMENTAL DETAILS

Barium manganese fluoride ($BaMnF_4$) exhibits a number of very interesting physical properties. At room temperature, the crystal has a layered orthorhombic structure [space group C_{2v}^{12} $(A2_1am)$] and lattice constants of $a=5.9845$ Å, $b=15.098$ Å, and $c=4.2216$ Å.[7] As seen in Fig. 1 the structure consists of layered sheets of linked $(MnF_6)^{4-}$ octahedra perpendicular to the b axis. The octahedra are distorted with average Mn-F distances of about 2.098 Å. The crystal is strongly piezoelectric and pyroelectric[8] and an incommensurate phase transition takes place below the critical temperature $T_c\sim 250$ K.[9] It becomes antiferromagnetically ordered at ~ 52 K; ordering is complete by ~ 26 K (Ref. 10) and the spins align along the b axis with a slight uncompensated component along c resulting in the existence of a very weak ferromagnetic moment in that direction.[11] At 4 K, antiferromagnetic and nuclear magnetic resonance experiments reveal a zone-center magnon energy of ~ 3 cm^{-1}. Magnetic data[12,13] agree with an exchange field $H_E\simeq 500$ kOe and a critical field for spin flopping when a magnetic field is applied along the b axis $H_c\simeq 9.8$ kOe. In the end, assuming only one single-ion anisotropy and neglecting interplane exchange interactions, neutron-diffraction results[9] lead to antiferromagnetic in-plane exchange integrals along the a and c directions given by $J_1=-3.17\pm 0.01$ cm^{-1} and $J_2=-4.55\pm 0.01$ cm^{-1}.

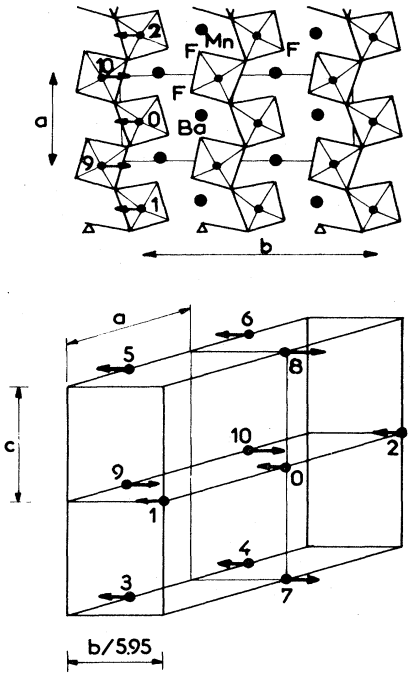

FIG. 1. Crystallomagnetic structure of $BaMnF_4$.

The sample of $BaMnF_4$ that we examined measures approximately $2\times3\times3$ mm^3 and was of good optical quality. Reference 6 treated the experimental conditions of optical excitation more extensively. The fluorescence signals were analyzed with the aid of a 1-m Hilger and Watts scanning monochromator (8 Å/mm in first order), detected with a RCA 31034-RF phototube and processed in an Ortec photon-counting system.

The samples could be cooled down to less than 2 K when immersed in superfluid helium with the help of a helium bath Ardin cryostat. The sample chamber of this cryostat was specially designed to fit in the magnet that we used, a Bitter-type split-coil electromagnet allowing us to obtain fields continuously up to about 125 kOe.

III. EXPERIMENTAL RESULTS

The low-temperature emission spectrum of $BaMnF_4$ is shown in Fig. 2. It consists of a broadband peaking around 6360 Å (Ref. 14) along with additional very weak structures appearing on its high-energy side.[6] Similar features were found on the low-energy side of the strongly π-polarized broad phonon-assisted excitation band peaking around 5200 Å; this is shown here again for clarity in the left part of the inset of Fig. 2. Doublets A_1/A_2 in excitation, A_1'/A_2' in emission were tentatively assigned to pure electronic transitions. The asymmetric sidebands noted A_3 and A_3' strongly resemble magnon sidebands; they could be associated with the pure excitons A_2 and A_2' with characteristic magnon frequency intervals of 37.2 and 39.2 cm^{-1}, respectively. These energy separations slightly differ from those given in Ref. 6: the reader has to retain the present ones since they result now from a

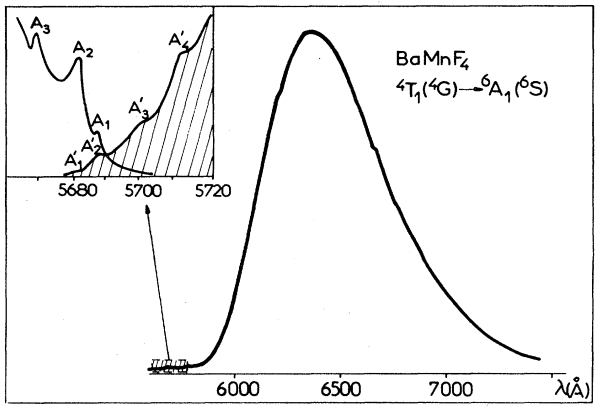

FIG. 2. Broadband emission and excitonic structures enlarged in the inset in excitation and in emission of $BaMnF_4$ at $T=2$ K.

careful substraction of the underlying background of both the phonon sidebands and the pure excitons. Line A_4' is seen as a phonon sideband of line A_2' with a characteristic phonon frequency of 81 cm^{-1}.[15]

In view of our analysis of the exciton dynamics, Fig. 3 shows the detailed time evolution of the A_2' exciton fluorescence. As opposed to that of the broadband, which is strictly exponential with a time constant of $\sim$49.5 ms, the A_2' exciton decay is made of two exponential components with time constants $\tau_f\simeq6$ ms and $\tau_s\simeq24$ ms. The weak A_1' exciton fluorescence decays with the time constant $\tau\simeq5.2$ ms.[6]

Figure 4 gathers the variations of the A_2' exciton decay rate τ_f^{-1}, deconvoluted at short times, and of the integrated emission intensity as a function of magnetic field. The intensity decreases and the decay rate increases quadratically with the applied field. The slow component of the exciton decay τ_s does not exhibit any appreciable change.

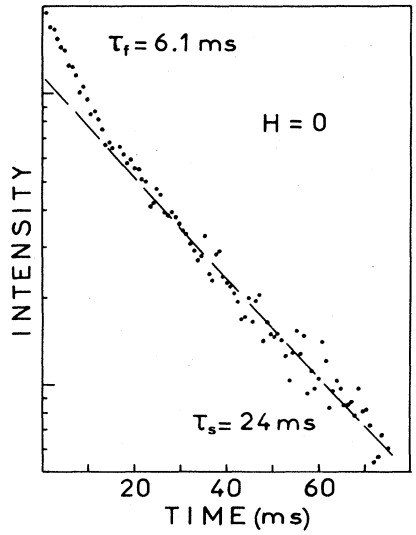

FIG. 3. Time evolution of the A_2' exciton fluorescence in $BaMnF_4$ at zero field and $T=2$ K.

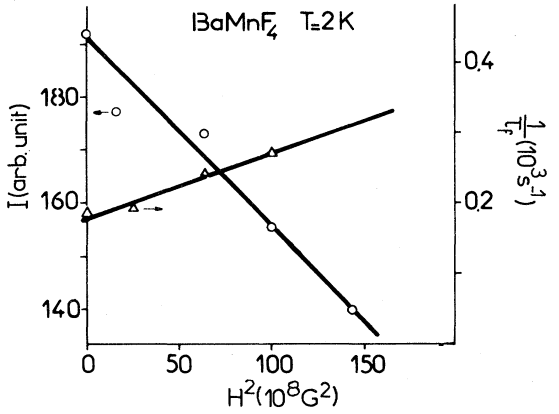

FIG. 4. Magnetic-field-induced variations of the exciton decay rate τ_f^{-1} (△) and of the integrated emission intensity (○).

IV. THEORETICAL INTERPRETATIONS

A. Definitions

At very low temperature, the cold magnon sidebands observed in absorption can be more or less intense and polarized depending on the crystal-site symmetry of the Mn^{2+} ions.[5] These transitions are attributed to the nondiagonal exchange-pair process proposed in the past[16,17] in which two near-neighbor manganese ions belonging to two distinct antiparallel magnetic sublattices are excited, one in a magnon state and the other in an exciton state.

In the case of the cold magnon sidebands observed in emission, two possible processes can be involved. One is attributed, as above, to a Tanabe-Moriya-Sugano ion-pair process in which an exciton is annihilated on one ion and a magnon is created on one of its nearest neighbors of the same magnetic sublattice. The other process is a single-ion process: it takes place within the same manganese ion and the exciton decays directly to the magnon state which is considered in the resulting transition.

In spite of these fundamental considerations, one obtains, however, the same formal expressions for the matrix elements of a single-ion or an ion-pair transition. Neglecting the dispersion of the exciton, which applies in most of the cases, these matrix elements transform as[5]

$$M_{k,\mu}=\sum_n e^{i\vec{k}\cdot\vec{r}_{on}}\vec{\mathscr{E}}\cdot\langle M^{\mu}_{A,n}\,|\,\vec{\mathrm{P}}\,|\,E_{A,o}\rangle \tag{1}$$

for ions o and n in the same sublattice A, and

$$N_{k,\mu}=\sum_m e^{i\vec{k}\cdot\vec{r}_{om}}\vec{\mathscr{E}}\cdot\langle M^{\mu}_{B,m}\,|\,\vec{\mathrm{P}}\,|\,E_{A,o}\rangle \tag{2}$$

for ions o and m in the opposite sublattices A and B. $\vec{\mathrm{P}}$ and $\vec{\mathscr{E}}$ stand for the electric dipole operator and the optical electric field, $|E\rangle$ and $|M\rangle$ for the electronic and magnetic wave functions. μ labels the various magnon branches.

The resulting expressions for the intensities of the cold magnon sidebands in emission and absorption are given by

$$E(\omega)=C\sum_{k\in BZ}\sum_{\mu}(|M_{k,\mu}|^2U^2_{k,\mu}+|N_{k,\mu}|^2V^2_{k,\mu})\times\delta(\hbar\omega-E_{\mathrm{exc}}+E^{\mu}_{\mathrm{mag}}(k))\,, \tag{3}$$

$$A(\omega)=C\sum_{k\in BZ}\sum_{\mu}(|N_{k,\mu}|^2U^2_{k,\mu}+|M_{k,\mu}|^2V^2_{k,\mu})\times\delta(\hbar\omega-E_{\mathrm{exc}}-E^{\mu}_{\mathrm{mag}}(k))\,. \tag{4}$$

Here E_{exc} and $E^{\mu}_{\mathrm{mag}}(k)$ are the exciton and magnon energies and $U_{k,\mu}$ and $V_{k,\mu}$ the canonical transformation coefficients of the magnon operators.

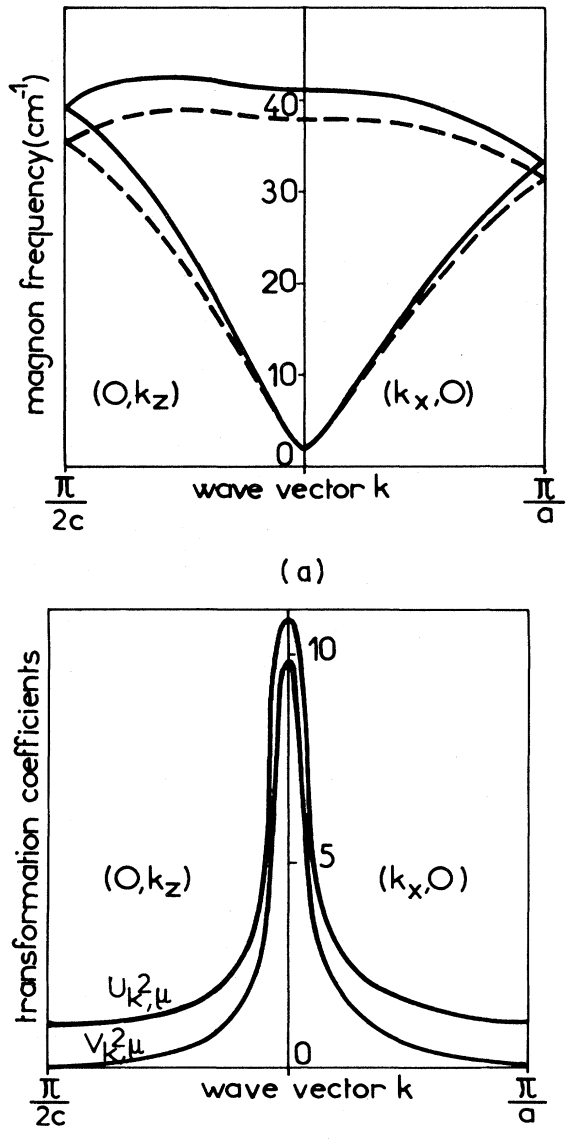

FIG. 5. (a) Dispersion curves for magnons in $BaMnF_4$ using $J_1=-3.2$ cm^{-1}, $J_2=-4.55$ cm^{-1}, $A=0.01$ cm^{-1} (following Ref. 9) (— — —); $J_1=-3.2$ cm^{-1}, $J_2=-5.3$ cm^{-1}, $A=0.01$ cm^{-1} (——). (b) Transformation coefficient $U^2_{k,\mu=+}$ and $V^2_{k,\mu=+}$ for magnons in $BaMnF_4$.

B. Magnon properties in $BaMnF_4$

Here we treat first the magnon density of states in $BaMnF_4$, considering only exchange interactions within the sheets perpendicular to the b axis of the crystal, then the form of the canonical transformation coefficients of the magnon operators. Assuming the same single-ion anisotropy H_A in each site, diagonalization of the total magnetic Hamiltonian by a standard method[18] enables us to obtain the following dispersion relations:

$$E_{\text{mag}}^{\mu=\pm}=2S[(A+J_1+J_2)^2-(J_1'\pm J_2')^2]^{1/2} . \tag{5}$$

The positive sign is for the acoustic branch and the negative sign is for the optical branch.

J_1 and J_2 are the superexchange integrals along the a and c directions and

$$A=\frac{g\mu H_A}{2S} , \tag{6}$$

$$J_1'=J_1\cos(k_x a/2) ,$$
$$J_2'=J_2\cos(k_z c) . \tag{7}$$

The dispersion curves along k_x and k_z in the first Brillouin zone (BZ) are shown in Fig. 5(a) using values from Ref. 9, i.e., $J_1=-3.2$ cm^{-1}, $J_2=-4.55$ cm^{-1}, and $A=0.01$ cm^{-1} and, also, using $J_2=-5.3$ cm^{-1} to be consistent with the exchange constant which is found in Rb_2MnF_4 where one deals with the same Mn-F-Mn geometry.[19]

The expressions for the transformation coefficients $U_{k,\mu}$ and $V_{k,\mu}$ used in the diagonalization above are given by

$$U_{k,\mu}^2=\frac{1}{2}\left[1+\frac{2S(J_1+J_2)}{E_m^{\mu}(k)}\right] ,$$
$$V_{k,\mu}^2=U_{k,\mu}^2-1 . \tag{8}$$

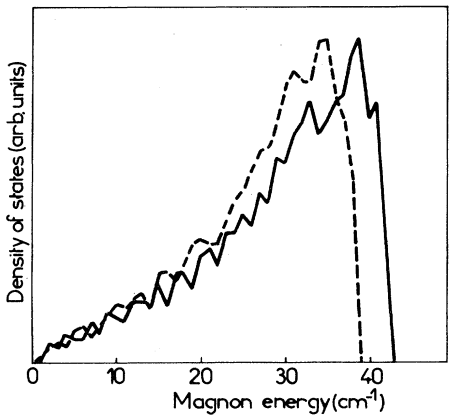

FIG. 6. Magnon density of states for $A=0.01$ cm^{-1}, $J_1=-3.2$ cm^{-1}, and $J_2=-4.55$ cm^{-1} (— — —) or $J_2=-5.3$ cm^{-1} (——).

A plot of $U_{k,\mu}^2$ and $V_{k,\mu}^2$ along k_x and k_z for $\mu=+$ is reported in Fig. 5(b). Near the BZ boundaries, $V_{k,\mu}^2\simeq 0$, so that the contribution of $N_{k,\mu}$ from the opposite sublattice ions appearing in (3) for the emission process, and, in absorption, the contribution of $M_{k,\mu}$ from the same sublattice ions appearing in (4), vanish at these points.

The magnon density of states for energies $E=E_{\text{mag}}^{\mu=+}(k)$, given by

$$\rho(E)=\sum_{k\in\text{BZ}}\delta(E-E_{\text{mag}}^{\mu=+}(k)) , \tag{9}$$

has been calculated using the two sets of values for J_1, J_2, and A reported above. The resulting curves shown in Fig. 6 are constructed from a histogram of the energies of the magnons given by (5) at 10^4 points evenly distributed throughout the Brillouin zone. Their maxima are displaced from each other by about 3.7 cm^{-1}.

C. Magnon sideband line shapes

Neglecting the interplane exchange interactions, the matrix elements M_k and N_k given by (1) and (2) become

$$M_k=P_1e^{ik_x a}+P_2e^{-ik_x a}+P_3\exp\left[i\left[k_x\frac{a}{2}+k_y\frac{b}{5.95}-k_z c\right]\right]+P_4\exp\left[i\left[-k_x\frac{a}{2}+k_y\frac{b}{5.95}-k_z c\right]\right]$$
$$+P_5\exp\left[i\left[k_x\frac{a}{2}+k_y\frac{b}{5.95}+k_z c\right]\right]+P_6\exp\left[i\left[-k_x\frac{a}{2}+k_y\frac{b}{5.95}+k_z c\right]\right] , \tag{10}$$

$$N_k=Q_1e^{-ik_z c}+Q_2e^{ik_z c}+Q_3\exp\left[i\left[k_x\frac{a}{2}+k_y\frac{b}{5.95}\right]\right]+Q_4\exp\left[i\left[-k_x\frac{a}{2}+k_y\frac{b}{5.95}\right]\right] , \tag{11}$$

where

$$P_i=\vec{\mathscr{E}}\cdot\langle M_{A,i}\,|\,\vec{\mathrm{P}}\,|\,E_{A,o}\rangle$$

and

$$Q_i=\vec{\mathscr{E}}\cdot\langle M_{B,i+6}\,|\,\vec{\mathrm{P}}\,|\,E_{A,o}\rangle . \tag{12}$$

Taking advantage of the symmetry relations among the pair transition moments P_i and Q_i by standard group theory

considerations and including polarization of light,[20] the intensity of the magnon sideband in emission can be written as

$$E^a(\omega)=\sum_{k\in BZ}\sum_{\mu}[a_1\cos^2(k_xa/2)\sin^2(k_zc)U^2_{k,\mu}+a_2\sin^2(k_zc)V^2_{k,\mu}]\delta(\hbar\omega-E_{exc}+E^{\mu}_{mag}(k)) \tag{13}$$

for $\vec{\mathscr{E}}\,||\,\vec{a}$,

$$E^b(\omega)=\sum_{k\in BZ}\sum_{\mu}b_1\sin^2(k_xa/2)\sin^2(k_zc)U^2_{k,\mu}\delta(\hbar\omega-E_{exc}+E^{\mu}_{mag}(k)) \tag{14}$$

for $\vec{\mathscr{E}}\,||\,\vec{b}$,

$$E^c(\omega)=\sum_{k\in BZ}\sum_{\mu}[c_1\sin^2(k_xa)+c_2\sin^2(k_xa/2)\cos^2(k_zc)]U^2_{k,\mu}+c_3\sin^2(k_xa/2)V^2_{k,\mu}\delta(\hbar\omega-E_{exc}+E^{\mu}_{mag}(k)) \tag{15}$$

for $\vec{\mathscr{E}}\,||\,\vec{c}$. We have excluded all terms which are of odd power in the trigonometric functions since they vanish when summed over k space.

Similar expressions are obtained for the magnon sideband in absorption by interchanging in the above $U^2_{k,\mu}$ and $V^2_{k,\mu}$ and replacing $E_{mag}(k)$ by $-E^{\mu'}_{mag}(k)$. For example,

$$A^a(\omega)=\sum_{k\in BZ}\sum_{\mu'}[a_2\sin^2(k_zc)U^2_{k,\mu'}+a_1\cos^2(k_xa/2)\sin^2(k_zc)V^2_{k,\mu'}]\delta(\hbar\omega-E_{exc}-E^{\mu'}_{mag}(k))\ . \tag{16}$$

A new magnon branch μ' is introduced to take into account the possible exciton-magnon interaction which usually reduces the energy spacing between the absorption magnon sideband and the exciton.[21] This effect, negligible in emission,[22] is approximately equivalent to a reduction of the number of near neighbor Mn^{2+} ions. This is brought about by rewriting the spin-wave energies,

$$E^{\mu'=\pm}_{mag}(k)=2S\left\{\left[A+\left[1-\frac{\alpha}{2}\right](J_1+J_2)\right]^2-\left[\left[1-\frac{\alpha}{2}\right](J'_1\pm J'_2)\right]^2\right\}^{1/2}\ . \tag{17}$$

The experimental magnon sidebands noted A_3 and A'_3 obtained after substraction of the background of the excitons and of the phonon sidebands are reported in Figs. 7 and 8. These curves are fitted with expressions (13)–(16) using the constants a_i,b_i and c_i,J_2, and α as adjustable parameters. The best agreement is obtained for (i) $J_2\simeq-5.3\ cm^{-1}$, for which we have reported in Fig. 6 the corresponding magnon density of states. (ii) $\alpha\simeq0.1$, which introduces the $2\text{-}cm^{-1}$ energy difference observed between the absorption and emission magnon peaks relative to the exciton positions.

The calculated line shapes result from a combination of the various polarization terms, in agreement with our unpolarized data. As a matter of fact, the π polarization of the A_3 magnon sideband correlates very well with the main contribution $\vec{\mathscr{E}}\,||\,c$ arising in the calculated profile. Both optical and acoustic magnon branches are included in the fitting of the emission magnon sideband whereas only the acoustic branch is necessary for the absorption data.

The main contributions are provided, in emission, from matrix elements between ion o and second-nearest neighbors in the same sublattice noted 3,4,5,6 in Fig. 1, and in absorption, from matrix elements between ion o and first-nearest neighbors in the opposite sublattices noted 9 and 10, thus for out-of-plane exchange couplings.

Since α can be defined in a simple way by $1-J'S'/JS$,

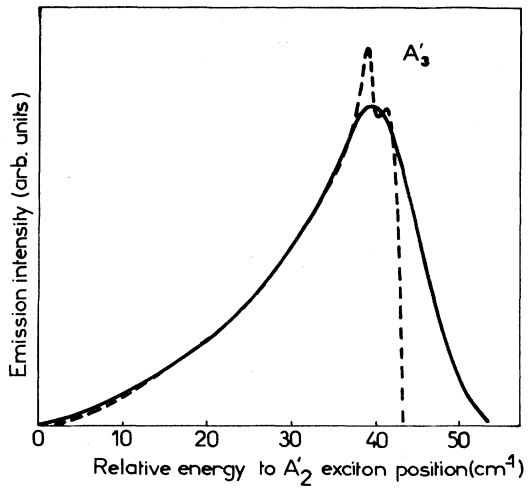

FIG. 7. A'_3 emission magnon sideband (——) observed and (— — —) calculated with respect to its A'_2 exciton origin.

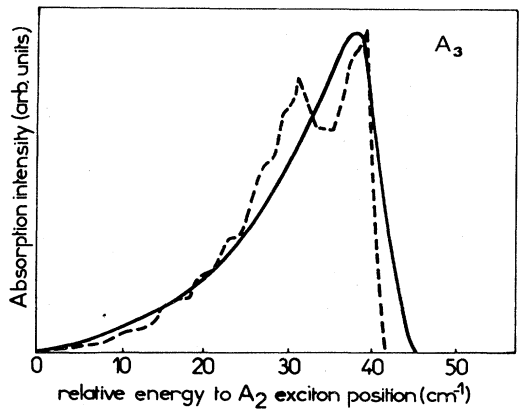

FIG. 8. A_3 absorption magnon sideband (——) observed and (— — —) calculated with respect to its A_2 exciton origin.

where J and J' stand for the effective exchange integrals in the fundamental and excited states, respectively, our estimation of α leads to the modified exchange integral $J'=1.5J$. A similar result has been found in MnF_2 (Ref. 23) and $CsMnF_3$ (Ref. 1): the excited-state value is greater than the value in ground state.

D. Exciton dynamics

The experimental data obtained previously indicated a quasicomplete self-localization of the excitons in the two-dimensional antiferromagnet $BaMnF_4$ at low temperature.[6] We would like to show here that this self-localization is a consequence of the crystal magnetic structure.

In most of the concentrated manganese compounds the exciton migrates in the crystal as a result of non-negligible short-range exchange interactions between ferromagnetically coupled nearest-neighbor manganese ions. Movement in the direction of antiferromagnetically coupled manganese ions is strongly inhibited since a large change ($\Delta M_s=2$) in the total spin projection would be needed. In $BaMnF_4$, we expect rather localized optical excitations, for the interplane displacements have to overcome very large interionic distances and the in-plane energy transfers to the nearest neighbor are concerned with antiparallel magnetic moments.

If such a conclusion is correct, a sufficiently strong magnetic field could change the magnetic structure of $BaMnF_4$ from antiferromagnetic to slightly ferromagnetic and bring about delocalization of the excitons. This would increase the exciton decay rate and decrease the overall intrinsic emission intensity. Figure 4 shows that this is actually what is found experimentally. This delocalization effect can be related to the magnetization data as follows.

The matrix element for an exchange-type excitation transfer between adjacent manganese ions belonging to different magnetic sublattices α and β is given by[24]

$$M^f_{\alpha,\beta}=\mathcal{M}^f_{\alpha,\beta}\cos^2\theta \quad \text{with } \theta=(\theta_\alpha-\theta_\beta)/2 , \tag{18}$$

where $\mathcal{M}^f_{\alpha,\beta}$ is an amplitude value independent of the orientations of the spins, f labels the electronic excitation which is considered, and θ stands for half the angle between the equilibrium positions of the spins on the ions α and β.

For fields higher than the critical field of the spin-flop transition, which is the case here since $H>H_c\sim 10$ kOe, one can write[1]

$$\cos\theta \propto \left[\frac{M}{M_0}\right] , \tag{19}$$

where M is the induced magnetization and M_0 its saturation value.

In case of incoherent optical excitations the energy-transfer rate P between ions α and β is proportional to the square of $M^f_{\alpha,\beta}$; it results in the following relationship:

$$P \propto \left[\frac{M}{M_0}\right]^4 . \tag{20}$$

At this point use is made of the molecular field theory to relate the induced magnetization to the applied magnetic field.

Introducing θ_H as the angle between H, the magnetic field, and the b axis of the crystal, the magnetization is given by[13,25]

$$M=\chi_\perp H[\sin^2(\theta_0+\theta_H)+\alpha\cos^2(\theta_0+\theta_H)] , \tag{21}$$

where θ_0 is the angle between the sublattice magnetizations and the b axis of the crystal, α is the ratio of parallel-to-transverse magnetic susceptibilities, and knowing that we find

$$\theta_0=\tfrac{1}{2}\tan^{-1}\{H^2\sin(2\theta_H)/[H_c^2-H^2\cos(2\theta_H)]\} . \tag{22}$$

Namely, provided that the applied magnetic field H is higher than the field for spin flopping H_c, when $H\perp b$ or $H||b$, i.e., $\theta_H=0$ or $\pi/2$, one obtains the simple relation

$$M\simeq\chi_\perp H . \tag{23}$$

Since $\chi_\perp\simeq M_0/(H_E+H_A)$, $H_E\gg H_A$, and $H_E\propto M$, we end with

$$H\propto\left[\frac{M}{M_0}\right]^2 . \tag{24}$$

Subsequently the exciton transfer rate should verify the following relationship:

$$P\propto H^2 . \tag{25}$$

This oversimplified uniaxial Neél model gives a good description of the observed magnetic-field-induced variations of the exciton decay rate τ_f^{-1} and of the integrated emission intensity shown in Fig. 4. This confirms the overall emission in $BaMnF_4$ as being entirely intrinsic and the exchange character of the interionic interactions which allow for the observed delocalization effect induced by the applied magnetic field.

V. CONCLUSION

The present line-shape analysis of the absorption and emission magnon sidebands A_3/A_3' clearly confirms their origins A_2/A_2' (and the corresponding resonant doublet A_1/A_1') as purely electronic transitions. Since the Mn^{2+} ions have noncentrosymmetric environments, the rather intense doublet A_1/A_2 can be attributed to electric dipole electronic transitions allowed through the admixtures of odd-parity crystal-field components in the $^4T_1$ excited-state wave functions. At the same time the absorption magnon sideband A_3 appears as a strong peak of comparable magnitude. Thus no reducing compensation effect seems to occur between the odd components resulting from a Tanabe-Moriya-Sugano (TMS) ion-pair process and those coming from the non-inversion symmetry as it does in CMC. The TMS ion-pair process can be involved solely.

The exchange parameters, which are deduced from our line-shape analysis, correlate very well with those obtained from the neutron-diffraction data and bring information about the excited-state exchange coupling and the dynamics of the collective optical and spin excitations as well.

We do not know very much about the origins of the A_1/A_2 optical doublet (crystal field, spin-orbit components, Jahn-Teller splitting, etc.); however, the antiferromagnetic coupling between the neighboring Mn^{2+} ions in the a and c planes and the large distance between the ions which are ferromagnetically coupled in the b direction qualitatively explain the quasilocalized character of the optical excitations, resulting in the rather long-lived exciton fluorescence decays $\tau'_{A_1} \simeq 5.2$ ms and $\tau_{A'_2} \simeq 6$ ms. This localization is not complete because of a slight ferromagnetic coupling along the c axis. Such a picture agrees in turn with the delocalization effect that we observe under magnetic field (through the appearance of enhanced ferromagnetic interion interactions).

It is concluded also that the emission line A'_1 can be attributed to a thermally activated transition (a hot exciton), and that the long-time constant of 24 ms, resulting from the decomposition of the A'_2 exciton fluorescence decay (into two components), can be attributed either to a residual contribution of the long-lived phonon sideband emission or to thermally activated shallow traps. Considering this decomposition, the data presented in Fig. 3 may appear to be consistent with the type of nonexponential decay analyzed in the paper on MnF_2 by Wilson *et al.*[26] and also in the paper on $CsMnF_3$ by Moncorgé *et al.*[1] However, in the case of $BaMnF_4$, the fit to the A'_2 exciton data of Fig. 3 with a similar biexcitonic process is not sufficiently satisfactory, which is not very surprising in consideration of the localized character of the optical excitations in this material. The fit is much better when the decay is expressed as the sum of two exponential components. In the end, further investigation is needed to clarify the nature of the exciton doublets A_1/A_2 (A'_1/A'_2) but the badly broadened lines and their restricted temperature range of observation should make this difficult.

ACKNOWLEDGMENTS

We would like to thank Drs. A. Linz and D. Gabbe for providing us with our sample and Professor B. Di Bartolo for initiating this research. Thanks are also expressed to the Service National des Champs Intenses (SNCI) for the high-magnetic-field facility and the Max Planck Institute, Grenoble, for all the necessary optical equipment.

[1] R. Moncorgé, B. Jacquier, C. Madej, and M. Blanchard, J. Phys. (Paris) 43, 1267 (1982), for instance.
[2] H. Yamamoto, D. S. McClure, C. Marzzacco, and M. Waldman, Chem. Phys. 22, 79 (1977).
[3] G. L. McPherson and A. H. Francis, Phys. Rev. Lett. 41, 1681 (1978).
[4] R. Ya. Bron, V. V. Eremenko, and E. V. Matyushkin, Fiz. Nizk. Temp. 5, 792 (1979) [Sov. J. Low Temp. Phys. 5, 314 (1979)].
[5] W. Jia, E. Strauss, and W. M. Yen, Phys. Rev. B 23, 6075 (1981).
[6] R. Moncorgé and B. Jacquier, Phys. Lett. 85A, 390 (1981).
[7] E. T. Keve, S. C. Abrahams, and J. L. Bernstein, J. Chem. Phys. 51, 4823 (1969).
[8] M. Eibschütz and H. J. Guggenheim, Solid State Commun. 6, 737 (1968).
[9] D. E. Cox, S. M. Shapiro, R. A. Cowley, M. Eibschütz, and H. J. Guggenheim, Phys. Rev. B 19, 5754 (1979).
[10] E. G. Spencer, H. J. Guggenheim, and G. J. Kominiak, Appl. Phys. Lett. 17, 300 (1970).
[11] E. L. Venturini and R. P. Morgenthaler, *Magnetism and Magnetic Materials—1974 (San Francisco),* Proceedings of the 20th Annual Conference on Magnetism and Magnetic Materials, edited by C. D. Graham, G. H. Lander, and J. J. Rhyne (American Institute of Physics, New York, 1975), Vol. 24, p. 168.
[12] S. V. Petrov, M. A. Popov, and L. A. Prozorova, Zh. Eksp. Teor. Fiz. 62, 1884 (1972) [Sov. Phys.—JETP 35, 981 (1972)].
[13] L. M. Holmes, M. Eibschütz, and H. J. Guggenheim, Solid State Commun. 7, 973 (1969); M. Eibschütz *et al.*, Phys. Rev. B 6, 2677 (1972).
[14] V. Goldberg, R. Moncorgé, D. Pacheco, and B. Di Bartolo, J. Lumin. 18/19, 143 (1979).
[15] V. V. Eremenko, A. P. Mokhn, YU. A. Popkov, and O. L. Reznitskaia, Uhr. Phys. J. 20, 144 (1975).
[16] K. Ueda and Y. Tanabe, J. Phys. Soc. Jpn. 48, 1137 (1980).
[17] Y. Tanabe, T. Moriya, and S. Sugano, Phys. Rev. Lett. 15, 1023 (1965).
[18] E. A. Turov, *Physical Properties of Magnetically Ordered Crystals* (Nauka, Moscow, 1963).
[19] R. A. Cowley, G. Shirane, R. J. Birgeneau, and H. J. Guggenheim, Physica 86/88B, 639 (1977).
[20] D. D. Sell, R. L. Greene, and R. M. White, Phys. Rev. 158, 489 (1967).
[21] J. B. Parkinson and R. Loudon, J. Phys. C 1, 1568 (1968).
[22] R. E. Dietz, A. E. Meixner, and H. J. Guggenheim, J. Lumin. 1/2, 279 (1970).
[23] W. M. Yen, G. F. Imbush, and D. L. Huber, in *Optical Properties of Ions in Crystals,* edited by H. M. Crosswhite and H. W. Moos (Interscience, New York, 1967), p. 301.
[24] V. V. Eremenko and E. G. Petrov, Adv. Phys. 26, 32 (1977).
[25] T. Nagamiya, K. Yosida, and R. Kubo, Adv. Phys. 4, 1 (1955).
[26] B. A. Wilson, J. Hegarty, and W. M. Yen, Phys. Rev. Lett. 41, 268 (1978).